ARTICLE

Encapsulating ^{111}In in Nanocontainers for Scintigraphic Imaging: Synthesis, Characterization, and *In Vivo* Biodistribution

Manuel M. Tsotsalas,[†,¶] Klaus Kopka,[‡,§,⊥,¶] Gianluigi Luppi,[†] Stefan Wagner,[‡,§] Marilyn P. Law,[‡,§] Michael Schäfers,[§,⊥] and Luisa De Cola[†,*]

[†]Physikalisches Institut and NRW Graduate School of Chemistry, Westfälische Wilhelms-Universität Münster, Mendelstrasse 7, D-48149 Münster, Germany, [‡]Klinik und Poliklinik für Nuklearmedizin, Universitätsklinikum Münster, Albert-Schweitzer-Strasse 33, D-48129 Münster, Germany, [§]Interdisciplinary Center of Clinical Research (IZKF Münster), Universität Münster, D-48149 Münster, Germany, and [⊥]European Institute of Molecular Imaging, Westfälische Wilhelms-Universität Münster, Mendelstrasse 11, D-48149 Münster, Germany. [¶]These authors contributed equally to this work.

ABSTRACT A new strategy for the radiolabeling of porous nanocontainers has been developed, and the first experiments *in vivo* are reported. Our approach consists of the use of nanometer-sized zeolites whose channels have been filled with the positively charged γ-emitter $^{111}In^{3+}$ *via* simple ion exchange. To avoid leaching of the isotope under physiological conditions, the entrances of the channels have been closed using a specifically designed molecular stopcock. This stopcock has a positively charged group that enters the channels and entraps the loaded radionuclides *via* electrostatic and steric repulsion. The other side of the stopcock is a bulky triethoxysilane group that can covalently bind to the walls of the zeolite entrances, thereby irreversibly closing the channels. The surface of the zeolites has been functionalized with different chemical groups in order to investigate the different biodistributions depending of the nature of the functionalizations. Preliminary *in vivo* experiments with Wistar rats have been performed and showed the potential of the approach. This strategy leads to a nanoimaging probe with a very high density of radioisotopes in a confined space, which is highly stable in physiological solution and could allow a large variety of functionalities on its external surface.

KEYWORDS: nanoparticle · zeolite L · scintigraphic imaging · stopper system · ^{111}In · *in vivo* imaging

Molecular imaging is the new frontier of medical diagnostics.[1] It aims at visualizing molecular systems or events occurring at the cellular or subcellular level, which are the "signatures" of a given disease. It represents, therefore, an outstanding breakthrough in the field of diagnostics currently provided in the clinical settings in terms of early diagnoses and in the efficient monitoring of therapeutic treatments. A major effort in this field is the design and development of new molecular probes which may improve the accuracy and the sensitivity of the detection. Among the most promising systems, nanomaterials are currently attracting the worldwide interest of researchers who aim to dedicate this technology to develop novel approaches in cancer imaging, molecular diagnosis, and targeted therapy.[2,3]

The investigated nanosystems include, among others, liposomes,[4,5] silica and silicon nanoparticles,[6−9] quantum dots,[10] micelles,[11] dendrimers,[12] and polymer-based nanoparticles.[13] The possibility of combining different imaging modalities in a single nanoparticle makes them very attractive for molecular imaging applications.[14,15]

This work presents a strategy for the preparation of nanosized materials, containing radioisotopes, which can be easily prepared, made water-soluble, and eventually target specific interactions. Our approach shows how a radionuclide, such as $^{111}In^{3+}$, can be entrapped inside narrow, subnanometer channels which belong to the nanocontainer, zeolite L, without any functionalization or coordination with any ligand. A strategy to close the channel entrances to avoid the leakage of the ions in physiological solution and to functionalize the surface with different chemical groups is described.[16,17] Finally, the different nanocontainers have been injected intravenously in Wistar rats and their biodistributions studied as a function of their surface functionalization.

In our group, we have already shown that micro- and nanometer zeolite L, a biocompatible crystalline aluminosilicate, can be functionalized, using different groups, leading to a dual probe contrast agent for MRI and optical imaging.[18] The possibility to also include a radiometal for scinti-

*Address correspondence to decola@uni-muenster.de.

Received for review September 5, 2009 and accepted December 1, 2009.

Published online December 18, 2009. 10.1021/nn901166u

© 2010 American Chemical Society

graphic imaging further shows how much potential these kinds of materials have for molecular imaging applications.

RESULTS AND DISCUSSION

Zeolite L is a biocompatible crystalline aluminosilicate in which corner-sharing SiO_4 and AlO_4 tetrahedra create a one-dimensional channel array. Free cations are present in the channels due to the negative charged aluminates. Since these systems are synthesized from bottom-up hydrothermal techniques, their size (30 nm up to several micrometers) and aspect ratio may be strictly controlled depending on the reaction conditions.[19] The zeolite crystals can be functionalized in different ways either by loading the channels[17,20] or by spatially controlling the covalent binding of functional groups.[16,21]

In this work, we have filled zeolite L nanocrystals with the radioisotope $^{111}In^{3+}$ in its ionic form and prevented its release by a specific functionalization of the channel entrances.

Zeolite L nanocrystals, due to their high porosity and charged interior, represent an attractive scaffold for cationic small molecules or ions, which can, without any chemical modification, be inserted into the channels. Such porosity represents an attractive feature because it offers a simple, straightforward, and fast approach to labeling the nanocrystals with cationic radionuclides or radiosynthons. Therefore, the insertion of the free ions into the nanostructures, which can be used as trapping agents, is the most desirable approach for the use of such nanomaterials for *in vivo* applications.

For our purpose, we have selected 30 × 30 nm crystals, which have been synthesized according to literature.[22] We have used unmodified zeolites, but also, to make the surface of the zeolite L crystals more hydrophilic,[23] a batch of the nanomaterials has been modified by covalent attachment of polyethylene glycol (PEG) moieties. The Si−OH groups of the surface of the zeolites reacted with the triethoxysilane derivative of the PEG molecules (Figure 1).

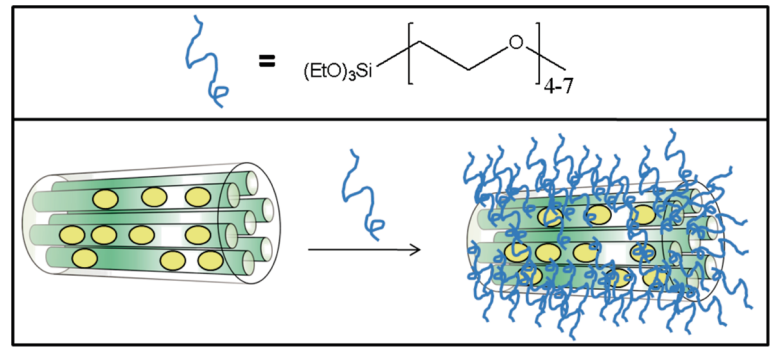

Figure 1. Schematic functionalization of the zeolite L surface with PEG.

The crystals were then loaded with the $^{111}In^{3+}$ ions by simple ion exchange with the K^+ ions present in the channels at the end of the synthesis (see Methods for details). The loading was assessed after centrifugation of the sample by measuring the radioactivity of the precipitate and the supernatant (precipitate = 98 MBq, supernatant = 13 MBq). The precipitate was then suspended in 0.9% NaCl solution and sonicated for 15 min. After centrifugation, the radioactivity of the precipitate and the supernatant was determined. We noticed that there is an exchange of the $^{111}In^{3+}$ ions with the Na^+ ions present in the physiological solution used, resulting in a leaking of the radioisotopes out of the zeolites. The leaking of the $^{111}In^{3+}$ from the channels was 11% in the first test (precipitate = 86 MBq, supernatant = 11 MBq). The procedure was repeated, and the leaking of the second test was 13% (precipitate = 72 MBq, supernatant = 11 MBq). The leakage continues if the solution is left standing for a day and is caused by the different cation concentration gradients across the entry to the channels ($[^{111}In^{3+}]_{in} > [^{111}In^{3+}]_{out}$ and $[Na^+]_{out} > [Na^+]_{in}$). In such conditions, we could not use the nanomaterials as a probe. We had to develop a strategy that would permanently entrap the ions inside the zeolite without modifying their properties and with a simple and fast reaction. We have, therefore, designed and synthesized a stopper molecule[16] that is able to close the channels permanently. Figure 2 depicts the strategy we have followed and shows the stopper molecule developed for this purpose.

The stopper molecule has been designed to fulfill several characteristics that would allow it to execute its function. A positively charged moiety, such as an imidazolium, must constitute one end of the stopper molecule in order to have a driving force for the insertion into the nanochannels[24,25] and to electrostatically repulse the positively charged indium ions. Furthermore, the tail should contain groups which could interact with the wall of the zeolites to stabilize the structure, such as urea derivatives. Finally, the head part of the stopper must contain a bulky group that is larger than the

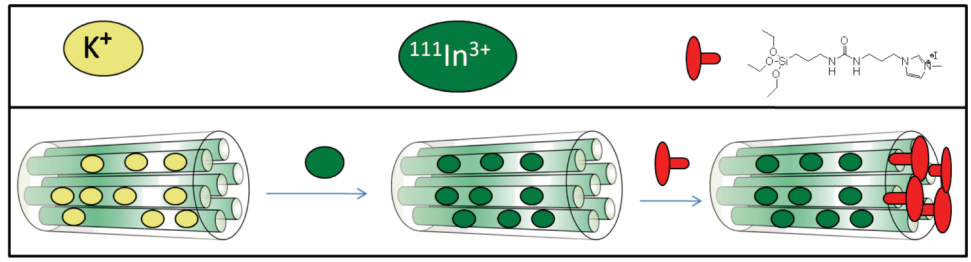

Figure 2. Radiolabeling of zeolite L nanocrystals and subsequent sealing using a positively charged stopcock.

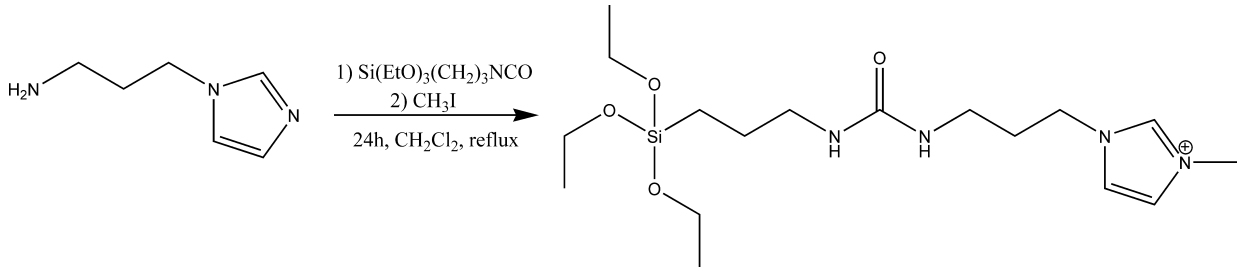

Scheme 1. Two-step three-component sequential one-pot reaction for the stopcock molecule synthesis.

channel entrance (0.71 nm) to avoid full insertion into the channels and terminated with highly reactive functional groups able to react with the surface of the channel entrances, such as silane systems.[26]

Therefore, the final formula of the stopper molecule possesses a bulky triethoxysilane moiety linked to an imidazolium salt *via* an alkyl urea spacer. The target compound was prepared by reacting corresponding amine with isocyanate to give urea, followed by *N*-alkylation with iodomethane to yield the imidazolium salt (see Scheme 1 and Methods for details).

After loading an unmodified and a PEG-modified zeolite samples with $^{111}In^{3+}$ ions by simple ion exchange, the nanomaterials were dried and suspended in a solution of stopper molecule in dry DMF. After reaction at 60 °C for 3 h, the samples were centrifuged and washed with EtOH. To check the stability of the closed radiolabeled nanocrystals in comparison to the open analogues (see above), a leaking test was performed again. The stopper-closed zeolites were stirred for 3 h in 0.9% NaCl solution and then were centrifuged. Afterwards, the amount of $^{111}In^{3+}$ ions exchanged by the Na^+ ions was determined by comparison of the radioactivity of the supernatant and the precipitate (unmodified zeolite sample, residue = 46.7 MBq, supernatant = 0.2 MBq, leaking = 0.4%; PEGylated zeolite sample, residue = 32.4 MBq, supernatant = 1.15 MBq, leaking = 4.4%). The leaking test was repeated after stirring overnight in 0.9% NaCl solution (unmodified zeolite sample, residue = 26.3 MBq, supernatant = 0.1 MBq, leaking = 0.4%; PEGylated zeolite sample, residue = 21.4 MBq, supernatant = 0.1 MBq, leaking = 0.5%).

After the second leakage test, the solids were suspended in 300 μL of 0.9% NaCl solution, and 150 μL of each solution was injected intravenously into individual male Wistar rats *via* the tail vein. At the same time, a solution of $[^{111}In]InCl_3$ with similar activity was injected into a male Wistar rat as a control experiment. Three rats (518−634 g) were used. Rat 1 received unmodified zeolites L filled with $^{111}In^{3+}$ and sealed with stopper molecule (10.3 MBq); rat 2 received 30 nm PEGylated zeolites L filled with $^{111}In^{3+}$ and sealed with stopper molecule (7.7 MBq); and rat 3 received $[^{111}In]InCl_3$ solution (10.7 MBq). Scintigraphic scanning was started at 70 min after injection of ^{111}In-labeled zeolites L and ^{111}In-labeled PEGylated zeolites L to obtain two static images (Figure 3a−d). Blood samples (6−7 per rat) were taken during the first 2 h from each rat (Figure 4a). To have a clear picture of uptake of the nanolabels by the organs, the rats were sacrificed immediately after the scan and tissues were removed to assess the biodistribution behavior of the tracers (Figure 4b).

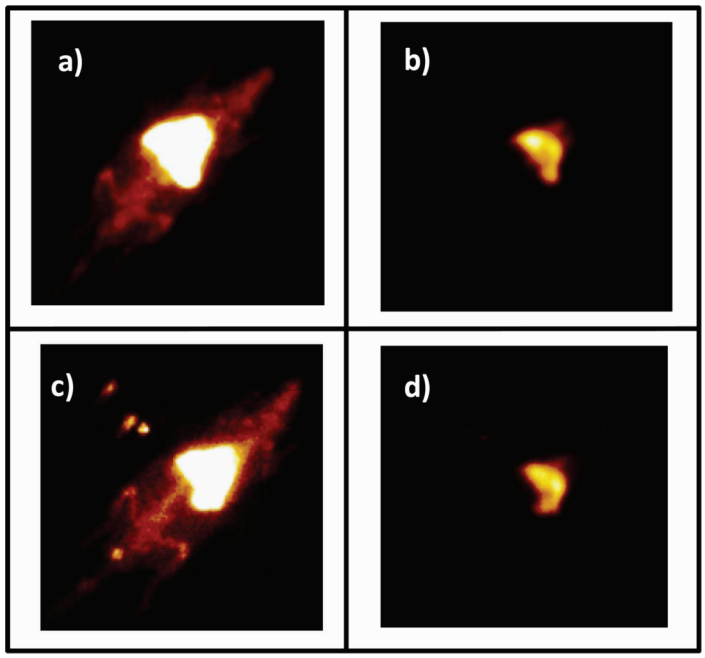

Figure 3. Two-dimensional static scintigraphic images of the rats 70 min after iv injection of the zeolite loaded with $^{111}In^{3+}$. Zeolite L injected into rat 1 in (a) high and (b) low contrast. Surface-modified (PEGylated) zeolite L injected into rat 2 in (c) high and (d) low contrast.

The images and the biodistribution results clearly show that the particles mainly accumulate in lung, liver, and spleen, while the free indium ions were observed mainly in blood and in the kidneys. The surface modification with PEG seems to only slightly influence the biodistribution behavior, which could be attributed to the chosen short chain length. As seen from the *in vivo* experiments, the particles behave as expected and as reported for similar systems in the literature.[27] The enhanced uptake in the liver and spleen is largely attributed to the macrophages residing in the tissues, which are responsible for clearing particles and macromolecules circulating in the blood. The stability of the particles seems to be very high *in vivo* because the distribution is very different from the distribution of the free

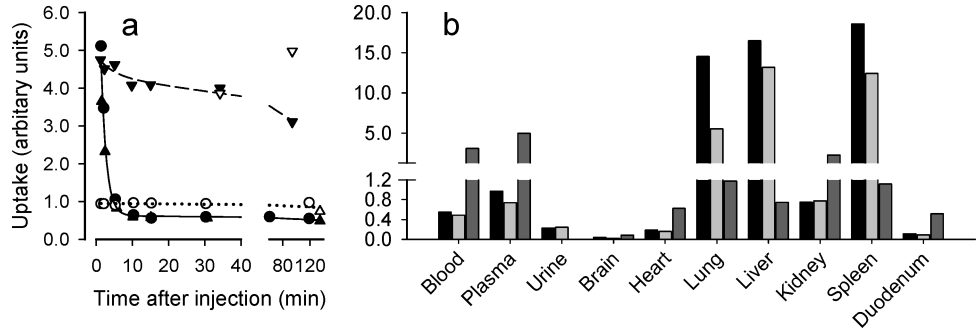

Figure 4. (a) Clearance of radioactivity from blood (solid symbols) and plasma (open symbols) of rats after iv injection of ^{111}In-labeled zeolite L or $^{111}InCl_3$. Six or seven blood samples were taken from each of three rats. Rat 1: 30 nm zeolites L filled with $^{111}In^{3+}$ and sealed with stopper molecule (●,○). Rat 2: 30 nm PEGylated zeolites L filled with $^{111}In^{3+}$ and sealed with stopper molecule (▲,△). Rat 3: free [^{111}In]$InCl_3$ (▼,▽). Solid line is the biexponential fit for blood, rats 1 and 2. Dashed line is the biexponential fit for blood, rat 3. Dotted line is the linear fit for plasma, rats 1 and 2. (b) Biodistribution of radioactivity in tissues of rats 100−130 min after iv injection of ^{111}In-labeled zeolites. Rat 1: 30 nm zeolites L filled with $^{111}In^{3+}$ and sealed with stopper molecule (black). Rat 2: 30 nm PEGylated zeolites L filled with $^{111}In^{3+}$ and sealed with stopper molecule (light gray). Rat 3: free [^{111}In]$InCl_3$ (gray).

indium ions. The calculated specific activities of the particles are 324 GBq/μmol for the unmodified zeolites and 224 GBq/μmol for the PEGylated zeolite sample (for the calculation, see Supporting Information).

The different activities are due most likely to a different content of the $^{111}In^{3+}$ ions inside the zeolites. In fact, the unmodified zeolite channels are more accessible than the PEGylated ones, allowing a better loading.

As a final step, the surface of the zeolite has been functionalized with azide moieties to test the possibility of attaching targeting molecules *via* simple and mild "click" chemistry. As a model compound, a triazole derivative has been synthesized by reaction of the azide group with propargyl alcohol (see Figure 5).

The 1,2,3-triazole-functionalized zeolites were obtained using a general route. First, the crystals were functionalized by a reaction of terminal Si−OH groups with 1-bromopropyl trichlorosilane. In the next step, the bromide was converted into an azide by substitution with NaN_3. In the last step, the triazole was formed by click reaction of the azide with the triple bond of the 2-propyn-1-ol. The reactions were followed by IR spectroscopy because the substitution of the bromide group by sodium azide is accompanied by the appearance of an intense N_3 absorption band at 2104 cm^{-1} typical of the asymmetrical stretching of the N_3 group. After reaction with propargyl alcohol, the N_3 absorption band disappears (see Supporting Information for the spectra).[28]

The triazole-functionalized zeolites were loaded with $^{111}In^{3+}$ and closed using the stopper molecule as described above, and the samples were injected into four male Wistar rats (316−346 g) intravenously *via* the tail vein. Blood samples were taken during the first hour (Figure 6a). The biodistribution of ^{111}In-labeled zeolites functionalized with triazole molecules was investigated by *ex vivo* dissection (4 rats) at 5 min, 20 min, 60 min, or 24 h post injection (Figure 6).

The experiment shows that the zeolites are rapidly cleared from blood and initially accumulated in the lung, liver, and spleen. Over time, the particles are cleared from the lung and the activity in spleen and kidney increased. Liver accumulation of the triazole-

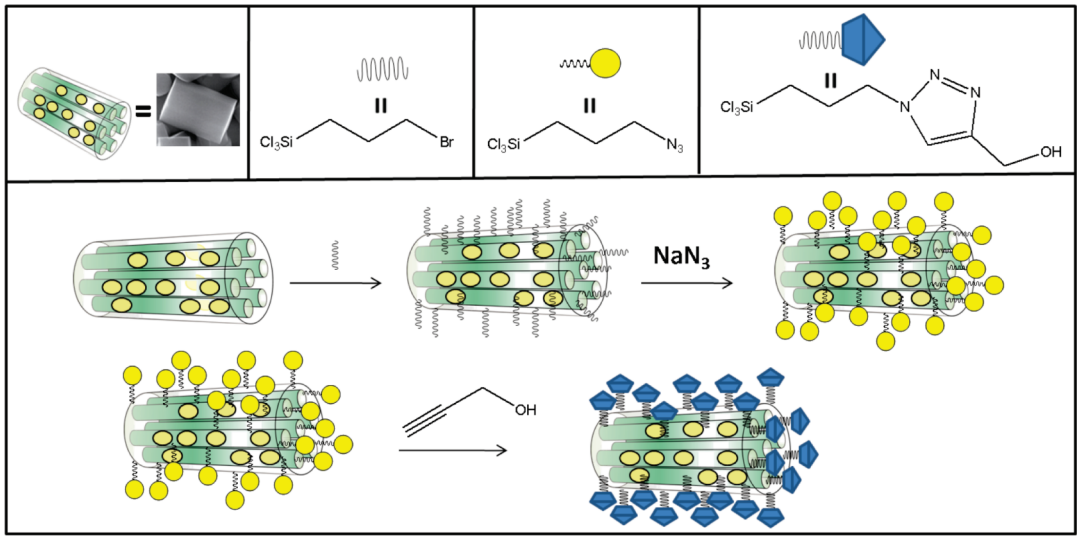

Figure 5. Surface functionalization of zeolite L nanocrystals with triazole molecules using "click chemistry".

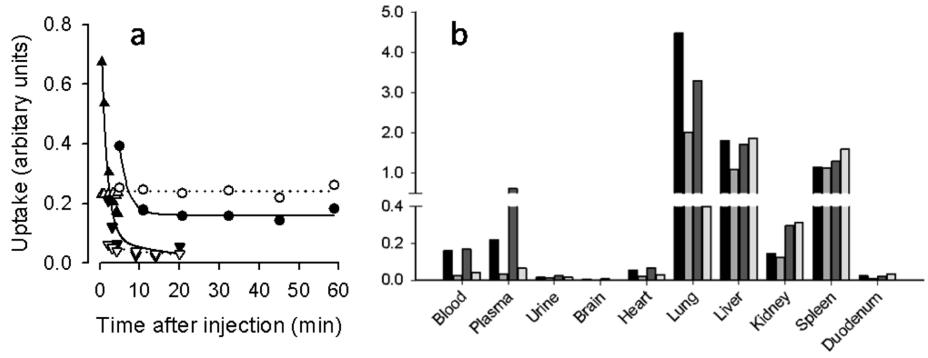

Figure 6. (a) Clearance of radioactivity from blood (solid symbols) and plasma (open symbols) of rats after iv injection of ^{111}In-labeled zeolites functionalized with triazole molecules. Six or seven blood samples were taken from each of three rats. Rat 1: *ex vivo* blood/plasma clearance at 20 s to 5 min (▲, △). Rat 2: at 1 to 20 min (▼, ▽). Rat 3: at 4 to 60 min (●,○). Solid lines are the biexponential fits for blood samples from rats 1, 2, or from rat 3. Dotted lines are the linear fits for corresponding plasma samples. (b) Biodistribution of radioactivity in tissues of rats after iv injection of ^{111}In-labeled zeolites functionalized with triazole molecules. Rat 1: 5 min (black). Rat 2: 20 min (medium gray). Rat 3: 60 min (dark gray). Rat 4: 24 h (light gray).

functionalized zeolite remained constant 24 h post-injection as compared to the initial uptake. This surface modification did not interfere with the loading of $^{111}In^{3+}$ and closing of the channels with the stopper molecule. Also, it was demonstrated that the zeolite surface can be modified *via* click chemistry under mild conditions. This paves the way for many functionalizations of the zeolite targeting biological structures such as receptors and enzymes. Experiments towards this direction are ongoing.

CONCLUSIONS

In conclusion, we have shown that the biocompatible zeolite L crystals can be filled with the radioisotope $^{111}In^{3+}$, a γ-emitter used for scintigraphic imaging in nuclear medicine, and closed using a tailor-made stopper molecule. The nanocontainers were prepared with very high specific activities of *ca.* 350 GBq/μmol, and almost no leaching of the loaded indium ions was detected after stopper closure of the channels. Surface functionalization of the zeolite L crystals before loading can be done either *via* direct coupling to the silanol groups on the surface or *via* click chemistry after azide functionalization of the zeolite surface. This last approach opens the development of very appealing and challenging new nanomaterials for multimodal molecular imaging applications and for selective targeting of desired systems.

METHODS

All reagents were obtained from Sigma-Aldrich and used as received if not specified otherwise. Pure zeolite L crystals were synthesized as described in ref 14; the potassium exchanged form was used for all experiments. 2-[Methoxy-(polyethyleneoxy)propyl]triethoxysilane (PEG-silane) and bromopropyl trichlorosilane were obtained from ABCR GmbH.

NMR spectra were recorded on an ARX 300 or an AMX 400 from Bruker Analytische Messtechnik (Karlsruhe, Germany). The ^{1}H NMR chemical shifts (δ) of the signals are given in parts per million and referenced to residual protons in the deuterated solvents dimethyl sulfoxide-d_6 (2.50 ppm) or methylene chloride-d_2 (5.32 ppm). The ^{13}C NMR chemical shifts are referenced to the chemical shift of the carbon in the deuterated solvents dimethyl sulfoxide-d_6 (39.5 ppm) or methylene chloride-d_2 (54 ppm). The signal splittings are abbreviated as follows: s, singlet; d, doublet; t, triplet; q, quartet; m, multiplet; bb, broadband. All coupling constants (*J*) are given in hertz (Hz). Mass spectrometry was performed in the Department of Organic Chemistry, University of Muenster. Electrospray ionization (ESI) mass spectra were recorded on a Bruker Daltonics (Bremen, Germany) MicroTof with loop injection. Isotopic distribution is given with abundance peak referred to the major isotope peak abundance (100%). FT-IR spectra were recorded on the Thermo Scientific Nicolet 380 FT-IR spectrometer (spectral range = 7800−350 cm^{-1} using the proprietary KBr beam splitter). The resolution was 2 cm^{-1}, and samples were prepared neat using NaCl crystal disks. Zeta potential measurements were recorded on a Zetasizer Nano ZS from Malvern instruments equipped with a 4 mW He−Ne, 633 nm laser.

Synthesis of the Stopper *N*-(3-Triethoxysilylpropyl)-*N'*-[3-(3-methyl-1*H*-imidazol-3-ium)propyl]urea iodine. The first step of the reaction between the aminopropyl imidazole and the triethoxysilylpropylisocyanate yields an almost quantitative formation of the urea intermediate as it is shown by the ESI-MS technique. The addition of iodomethane leads to the formation of the imidazolium salt with 95% yield and high purity.[29] Due to the reactivity of the silyl moieties that can result in the formation of undesired side products during the purification procedure, a simple and fast workup procedure of the target compound was chosen.[30,31] Therefore, the freshly prepared stopcock was precipitated by Et_2O and characterized by NMR, IR spectroscopy, and mass spectrometry and used without further purification.

In a PTFE round-bottom flask, aminopropyl imidazole (4 mmol, 0.47 mL) was dissolved in DCM (10 mL), and triethoxysilylpropylisocyanate (4 mmol, 0.99 mL) was added dropwise. The solution was stirred at reflux temperature for 1 h. Afterward, a solution of iodomethane (8.28 mmol, 0.5 mL) in DCM (2 mL) was added. The solution was stirred at reflux temperature for a further 2 h and the solvent evaporated under reduced pressure, yielding a light yellow-brown dense oil (1.47 g, 3.8 mmol, yield = 95% by NMR). In order to avoid hydrolysis of the stopper molecule, fast purification was achieved by precipitation by adding Et_2O (0.5 mL) to the crude mixture. The white precipitate was isolated by centrifugation (4500 rpm, 10 min), dried under reduced pressure, and characterized by NMR, IR, and ESI-Tof techniques. Small amounts of unreacted imidazole adduct (*m/z* = 373.2264) and monohydrolyzed product (*m/z* = 359.2104) were

detected. ^{1}H NMR shows the presence of reaction solvent (CH_2Cl_2, $\delta = 5.75$), which was hard to remove under vacuum, probably due to strong molecular interactions. ^{13}C NMR was recorded in CD_2Cl_2 in order to increase the stopper stability during the measuring time. Presence of DMSO-d_6 (10% v/v) was, however, necessary in order to increase the compound solubility.

Light yellow-brown dense oil: ^{1}H NMR (400 MHz, DMSO-d_6) $\delta = 0.50$ (m, 2H, CH_2), 1.13 (t, 9H, $J = 8$ Hz, 3 CH_3), 1.39 (m, 2H, CH_2), 1.84 (m, 2H, CH_2), 2.93 (m, 2H, CH_2), 2.96 (m, 2H, CH_2), 3.73 (q, $J = 8$ Hz, 6H, 3 CH_2), 3.85 (s, 3H, CH_3), 4.15 (t, $J = 8$ Hz, 2H, CH_2), 5.94 (bb, 2H, NH), 7.71 (s, 1H, CH), 7.79 (s, 1H, CH), 9.13 (s, 1H, CH); ^{13}C NMR (100 MHz, CD_2Cl_2 (10% v/v DMSO-d_6)) $\delta = 8.1$, 18.6, 24.2, 31.4, 36.0, 37.1, 43.1, 47.7, 58.7, 123.25, 123.84, 137.5, 159.5; IR (neat) $\nu = 3316$ (NH), 3145, 3088, 2971, 2929, 2884, 1694 (CO), 1561 cm^{-1}; HRMS (MS-ESI-Tof) *m/z* calcd for $C_{17}H_{35}N_4O_4Si$ $(M)^+ = 387.2428$, found $= 387.2424$.

Loading of the Zeolites with Indium Ions. One milligram of zeolite sample was added into a centrifuge tube and suspended in 1 mL of the [^{111}In]$InCl_3$ solution ($A = 224-367$ MBq, GE Healthcare Buchler, Braunschweig, Germany). Because the [^{111}In]$InCl_3$ solution is acidic (0.04 N HCl, $V = 500$ μL) and the protons would interfere with the loading process, the solution was neutralized using tetrapentyl ammonium hydroxide (30 μmol, $V = 38$ μL of a 20%(T) solution in water, Fluka, Germany) and further diluted with 462 μL of water for injection (BBraun). After sonication for 15 min at 60 °C, the suspension was centrifuged for 15 min at 12 000 rotations/min (Centrifuge 5415D, Eppendorf, Germany). The supernatant was pipetted off, and the activities of the precipitate and the supernatant were determined. Afterwards, the sample was dried in an oven and transferred with DMF (3 × 1.5 mL) into a Teflon tube.

Synthesis of the Zeolite Functionalized with PEG. Thirty milligrams of potassium exchanged zeolite L crystals was suspended in 5 mL of dry DMF, and 30 μL of PEG-silane was added. After stirring for 3 h at 70 °C, the sample was centrifuged and washed twice with EtOH. Afterward, the zeta potential was measured in two different buffer systems (0.1 M acetate buffer pH 4.7 (AC47); 0.1 M phosphate buffer pH 7(PP70)). The zeta potential changes due to the different surface modifications. The unfunctionalized zeolite crystals have a zeta potential of −20.2 (AC4.7) and −28.2 (PP70). The zeolite crystals functionalized with PEG have a zeta potential of −5.4 (AC47) and −12.2 (PP70).

Synthesis of the Zeolite Functionalized with Triazole Molecules. Twenty milligrams of potassium exchanged zeolite L crystals was suspended in 5 mL of dry DMF in a Teflon centrifuge tube, and 20 μL of bromopropyl trichlorosilane was added. After sonication for 15 min and stirring for 3 h at 60 °C, the sample was centrifuged and washed with EtOH twice. In the next step, NaN_3 (15 mg, 0.23 mmol) was added to the zeolite in 5 mL of DMF and stirred at room temperature overnight. Afterward, the sample was centrifuged and washed with water twice. In the last step, 2 mL of propargyl alcohol was added to the azide-terminated zeolite in 5 mL of H_2O and heated to 70 °C for 5 days.

The NaN_3-functionalized zeolites have a zeta potential of −21.5 (AC47) and −35.4 (PP70). After reaction with propargyl alcohol, the zeta potential is −11.6 (AC4.7) and −31.4 (PP70).

Closure of the Zeolite. A solution of 1 mg (2.6 μmol) of stopper molecule in 1.5 mL of DMF was added to the $^{111}In^{3+}$-loaded zeolite sample in 1.5 mL of DMF and stirred at 60 °C for 3 h. After centrifugation for 30 min at 4000 rotations/min (Centrifuge Sigma 3K-1, Germany), the supernatant was pipetted off and the activities of the precipitate and the supernatant were determined. After washing with 0.9% NaCl solution, the sample was stirred overnight in 0.9% NaCl (BBraun) solution. Afterwards, the sample was injected into the rats.

Biobistribution Experiments. ***Animals.*** Studies were approved by the federal animal rights committee and were performed in accordance with institutional guidelines for health and care of experimental animals.

Male Wistar rats (316−634 g) were anaesthetized by inhalation (isoflurane 2%, oxygen 0.5 L · min^{-1}) for insertion of indwelling catheters into the ventral tail artery (for blood sampling) and one lateral tail vein (for injection of ^{111}In-labeled zeolites). Animals were allowed to recover for 1−2 h under light restraint. *Ex vivo* biodistribution studies were carried out in conscious animals.[32] Rats were re-anaesthetized for scintigraphic imaging.

Indwelling catheters were not used for 24 h studies. Instead, a cannula (BD VasculonPlus, 24 GA) was inserted into a tail vein under anesthesia for injection of ^{111}In-labeled zeolites and was removed after injection.

***Ex Vivo* Biodistribution Studies.** ^{111}In-labeled zeolites (2.5−11 MBq) in 0.9% NaCl (0.15−0.55 mL) were injected *via* the tail vein. Six or seven sequential arterial blood samples (*ca.* 100 μL) were taken. An aliquot of whole blood was taken and the remainder centrifuged to separate the plasma. Rats were sacrificed by intravenous injection of sodium pentobarbitone (Euthatal) at 200 mg · (kg body weight)$^{-1}$ at 5 min to 24 h after injection. Blood was taken by cardiac puncture, and tissues were rapidly removed. Tissue samples were blotted dry using filter paper and transferred to weighed vials for reweighing and measurement of radioactivity using an automated gamma counter (Wallac Wizard 3′′, Perkin-Elmer Life Sciences, Boston, MA). Radioactivity was expressed as cps · (g wet tissue)$^{-1}$.

As the error associated with pipetting small volumes (10 μL) of the injected ^{111}In-labeled zeolite suspension was large, the radioactivity in each injection syringe was measured (ion chamber Aktivimeter ISOMED 2000, Nuklear-Medizintechnik Dresden GmbH, Germany) before and after injection into each rat and the injected dose expressed as kBq · kg^{-1}. To compare tissue uptake in different animals, results were expressed as uptake (arbitrary units), defined as

$$\text{uptake} = \frac{\text{tissue radioactivity (cps)/tissue wet weight (g)}}{\text{radioactivity injected (kBq)/body weight (kg)}}$$

Scintigraphic Scanning. Single rats were scanned by planar scintigraphy using one detector of a MultiSPECT M3 gamma camera (Siemens) with the medium energy (ME) collimator operating at zoom 1.0. Rats were anaesthetized 10 min before scan start, and anesthesia was maintained throughout the scan (isoflurane 2%, oxygen 0.5 L · min^{-1} per rat). ^{111}In-labeled zeolites were injected *via* a venous catheter either 70 min before scan start (conscious animals) or at scan start (anaesthetized rat positioned in the scanner). Blood samples were taken from some rats during the scan.

Acknowledgment. This work was supported by grants from the Deutsche Forschungsgemeinschaft (DFG), Sonderforschungsbereich (SFB) 656, Münster, Germany (Projects A2 and A3). We are grateful to the NRW Graduate School of Chemistry at Münster (GSC-MS) for a Ph.D. stipend for M.T., and G.L. thanks the Bundesministerium für Bildung und Forschung−BMBF India project No. 03 × 0015C India−for the grant and the Dr. H. Luftmann's group for the helpful consultations and the exact mass measurements. We also wish to thank Fond der Chemischen Industrie for financial support.

Supporting Information Available: Calculation of the specific activity of the ^{111}In-filled zeolite samples. FT-IR spectra of the azide and triazole-functionalized zeolite. Exact mass, NMR, and FT-IR spectra of the stopper molecule. This material is available free of charge *via* the Internet at http://pubs.acs.org.

REFERENCES AND NOTES

1. Weissleder, R. Molecular Imaging in Cancer. *Science* **2006**, *312*, 1168–1171.
2. Hamoudeh, M.; Kamleh, M.; Diab, R.; Fessi, H. Radionuclides Delivery Systems for Nuclear Imaging and Radiotherapy of Cancer. *Adv. Drug Delivery Rev.* **2008**, *60*, 1329–1346.
3. Sanhai, W.; Sakamoto, J.; Canady, R.; Ferrari, M. Seven Challenges for Nanomedicine. *Nat. Nanotechnol.* **2008**, *3*, 242–244.
4. Mulder, W.; Douma, K.; Koning, G.; Van Zandvoort, M.; Lutgens, E.; Daemen, M.; Nicolay, K.; Strijkers, G. Liposome-Enhanced MRI of Neo-intimal Lesions in the ApoE-KO Mouse. *Magn. Reson. Med.* **2006**, *55*, 1170–1174.

5. Mulder, W.; Strijkers, G.; Griffioen, A.; van Bloois, L.; Molema, G.; Storm, G.; Koning, G.; Nicolay, K. A Liposomal System for Contrast-Enhanced MR Imaging of Molecular Targets. *Bioconjugate Chem.* **2004**, *15*, 799–806.
6. Erogbogbo, F.; Yong, K.; Roy, I.; Xu, G.; Prasad, P.; Swihart, M. Biocompatible Luminescent Silicon Quantum Dots for Imaging of Cancer Cells. *ACS Nano* **2008**, *2*, 873–878.
7. Piao, Y.; Burns, A.; Kim, J.; Wiesner, U.; Heyeon, T. Designed Fabrication of Silica-Based Nanostructured Particle Systems for Nanomedicine Applications. *Adv. Funct. Mater.* **2008**, *18*, 3745–3758.
8. Rosso-Vasic, M.; Spruijt, E.; Popovic, Z.; Overgaag, K.; van Lagen, B.; Grandidier, B.; Vanmaekelbergh, D.; Dominguez-Gutierrez, D.; De Cola, L.; Zuilhof, H. Amine Terminated Silicon Nanoparticles: Synthesis, Optical Properties and Their Use in Bioimaging. *J. Mater. Chem.* **2009**, *19*, 5926–5933.
9. Tasciotti, E.; Liu, X.; Bhavane, R.; Plant, K.; Leonard, A.; Price, B.; Cheng, M.; Decuzzi, P.; Tour, J.; Robertson, F.; Ferrari, M. Mesoporous Silicon Particles as a Multistage Delivery System for Imaging and Therapeutic Applications. *Nat. Nanotechol.* **2008**, *3*, 151–157.
10. Woodward, J.; Kennel, S.; Mirzadeh, S.; Dai, S.; Wall, J.; Richey, T.; Avenell, J.; Rondinone, A. *In Vivo* SPECT/CT Imaging and Biodistribution Using Radioactive Cd125mTe/ZnS Nanoparticles. *Nanotechnology* **2007**, *18*, 175103–175108.
11. Accardo, A.; Tesauro, D.; Roscigno, P.; Gianolio, E.; Paduano, L.; D'Errico, G.; Pedone, C.; Morelli, G. Physicochemical Properties of Mixed Micellar Aggregates Containing CCK Peptides and Gd Complexes Designed as Tumor Specific Contrast Agents in MRI. *J. Am. Chem. Soc.* **2004**, *126*, 3097–3107.
12. Kobayashi, H.; Koyama, Y.; Barrett, T.; Hama, Y.; Regino, C.; Shin, I.; Jang, B.; Le, N.; Paik, C.; Choyke, P.; *et al.* Multimodal Nanoprobes for Radionuclide and Five-Color Near-Infrared Optical Lymphatic Imaging. *ACS Nano* **2007**, *1*, 258–264.
13. Cho, Y.; Park, S.; Han, T.; Son, D.; Park, J.; Oh, S.; Moon, D.; Cho, K.; Ahn, C.; Byun, Y.; *et al. In Vivo* Tumor Targeting and Radionuclide Imaging with Self-Assembled Nanoparticles: Mechanisms, Key Factors, and Their Implications. *Biomaterials* **2007**, *28*, 1236–1247.
14. Cheon, J.; Lee, J. Synergistically Integrated Nanoparticles as Multimodal Probes for Nanobiotechnology. *Acc. Chem. Res.* **2008**, *41*, 1630–1640.
15. Park, K.; Lee, S.; Kang, E.; Kim, K.; Choi, K.; Kwon, I. New Generation of Multifunctional Nanoparticles for Cancer Imaging and Therapy. *Adv. Funct. Mater.* **2009**, *19*, 1553–1566.
16. Huber, S.; Calzaferri, G. Sequential Functionalization of the Channel Entrances of Zeolite L Crystals. *Angew. Chem., Int. Ed.* **2004**, *43*, 6738–6742.
17. Calzaferri, G.; Lutkouskaya, K. Mimicking the Antenna System of Green Plants. *Photochem. Photobiol. Sci.* **2008**, *7*, 879–910.
18. Tsotsalas, M.; Busby, M.; Gianolio, E.; Aime, S.; De Cola, L. Functionalized Nano-Containers as Dual, Magnetic and Optical, Probes for Molecular Imaging Applications. *Chem. Mater.* **2008**, *20*, 5888–5893.
19. Ruiz, A.; Brühweiler, D.; Ban, T.; Calzaferri, G. Synthesis of Zeolite L. Tuning Size and Morphology. *Monatsh. Chem.* **2005**, *136*, 77.
20. Calzaferri, G. Zeolite Microcrystals as Hosts for Supramolecular Organization of Dye Molecules. *Chimia* **1998**, *52*, 525–532.
21. Busby, M.; Kerschbaumer, H.; Calzaferri, G.; De Cola, L. Orthogonally Bi-Functional Fluorescent Zeolite-L Micro-Crystals. *Adv. Mater.* **2008**, *20*, 1614–1618.
22. Tsapatsis, M.; Lovallo, M.; Okubo, T.; Davis, M.; Sadakata, M. Characterization of Zeolite-I Nanoclusters. *Chem. Mater.* **1995**, *7*, 1734–1741.
23. Li, H.; Devaux, A.; Popovic, Z.; De Cola, L.; Calzaferri, G. Carboxyester Functionalizad Dye Zeolite L Host Guest Materials. *Microporous Mesoporous Mater.* **2006**, *95*, 112–117.
24. Maas, H.; Khatyr, A.; Calzaferri, G. Phenoxazine Dyes in Zeolite L, Synthesis and Properties. *Microporous Mesoporous Mater.* **2003**, *65*, 233–242.
25. Megelski, S.; Lieb, A.; Pauchard, M.; Drechsler, A.; Glaus, S.; Debus, C.; Meixner, B.; Calzaferri, G. Orientation of Fluorescent Dyes in the Nano Channels of Zeolite L. *J. Phys. Chem. B* **2001**, *105*, 25–35.
26. Ban, T.; Bruehweiler, D.; Calzaferri, G. Selective Modification of the Entrances of Zeolite L with Triethoxysilylated Coumarin. *J. Phys. Chem. B* **2004**, *108*, 16348–16352.
27. Li, S.; Huang, L. Targeted Delivery of Antisense Oligodeoxynucleotide and Small Interference RNA into Lung Cancer Cells. *Mol. Pharmaceutics* **2008**, *5*, 579–588.
28. Lummerstorfer, T.; Hoffmann, H. Click Chemistry on Surfaces: 1,3-Dipolar Cycloaddition Reactions of Azide-Terminated Monolayers on Silica. *J. Phys. Chem. B* **2004**, *108*, 3963–3966.
29. Cazin, C.; Veith, M.; Braunstein, P.; Bedford, R. Versatile Methods for the Synthesis of Si(OR)(3)-Functionalised Imidazolium Salts, Potential Precursors for Heterogeneous NHC Catalysts and Composite Materials. *Synthesis* **2005**, *4*, 622–626.
30. Gadenne, B.; Hesemann, P.; Moreau, J. Supported Ionic Liquids: Ordered Mesoporous Silicas Containing Covalently Linked Ionic Species. *Chem. Commun.* **2004**, 1768–1769.
31. Lee, B.; Im, H.-J.; Luo, H.; Hagaman, E.; Dai, S. Synthesis and Characterization of Periodic Mesoporous Organosilicas as Anion Exchange Resins for Perrhenate Adsorption. *Langmuir* **2005**, *21*, 5372–5376.
32. Law, M. Demonstration of the Suitability of CGP 12177 for *In Vivo* Studies of β-Adrenoceptors. *Br. J. Pharmacol.* **1993**, *109*, 1101–1109.